

# An Adherent Raindrop Detection Method Using MSER

Koichi Ito\*, Kazumasa Noro\* and Takafumi Aoki\*

\* Graduate School of Information Sciences, Tohoku University,

6-6-05, Aramaki Aza Aoba, Sendai, 980-8579 Japan.

E-mail: ito@aoki.ecei.tohoku.ac.jp

**Abstract**—Image processing algorithms used in surveillance systems are designed to work under good weather conditions. For example, in a rainy day, raindrops are adhered to camera lenses and windshields, resulting in partial occlusions in acquired images, and making performance of image processing algorithms significantly degraded. To improve performance of surveillance systems in a rainy day, raindrops have to be automatically detected and removed from images. Addressing this problem, this paper proposes an adherent raindrop detection method from a single image which does not need training data and special devices. The proposed method employs image segmentation using Maximally Stable Extremal Regions (MSER) and qualitative metrics to detect adherent raindrops from the result of MSER-based image segmentation. Through a set of experiments, we demonstrate that the proposed method exhibits efficient performance of adherent raindrop detection compared with conventional methods.

## I. INTRODUCTION

Surveillance systems are used to detect, recognize and track objects from video sequences and understand their behaviors such as access control security, person identification at a distance, crowd flux statistics, anomaly detection and alarming, traffic surveillance, etc. [1]. Although the surveillance systems are mostly used in outdoor situations, image processing algorithms used in surveillance systems are designed to work under good weather conditions. For example, in a rainy day, raindrops are adhered to camera lenses and windshields. Such adherent raindrops result in partial occlusions in acquired images, making performance of image processing algorithms significantly degraded. To improve performance of surveillance systems in a rainy day, raindrops have to be automatically detected and removed from images. In this paper, we focus on detecting adherent raindrops in an image.

There are some works on raindrop detection. Garg and Nayar [2] analyzed physical properties of rain, modeled rain by its dynamics and photometry and detected it from videos. Zhang et al. [3] extended the rain streak detection approach [2] by using both temporal and chromatic properties of rain in video. Barnum et al. [4] developed a model of the shape and appearance of a single rain streak. Kang et al. [5] removed rain streaks using a single image. The above works aimed to detect falling raindrops whose properties are significantly different from those of adherent raindrops.

Kurihata et al. [6] proposed an adherent raindrop detection method using principal component analysis, called eigendrop.

Wu et al. [7] generated a raindrop saliency map by analyzing color, texture and shape characteristics of raindrops and detected raindrops using the saliency map. Halimeh and Roser [8] and Roser and Geiger [9] developed a photometric model of adherent raindrops and detected adherent raindrops from video sequences using the model. You et al. [10] also modeled adherent raindrops and detected raindrops based on the motion and the intensity temporal derivatives of video sequences. Yamashita et al. [11] detected raindrops based on the difference between stereo images. Yamashita et al. [12] also detected raindrops using a moving camera. The adherent raindrop detection methods mentioned above need training data, video sequences or special devices, resulting in the limited range of applications.

Addressing the above problem, we propose an adherent raindrop detection method from a single image which does not need training data and special devices. The proposed method employs image segmentation using Maximally Stable Extremal Regions (MSER) [13] and qualitative metrics to detect adherent raindrops from the result of MSER-based image segmentation. Through a set of experiments, we demonstrate that the proposed method exhibits efficient performance of adherent raindrop detection compared with conventional methods.

## II. RAINDROP DETECTION METHOD

An adherent raindrop on the glass surface in front of a camera becomes a local fish-eye lens refracting light from a wide range of angles into the camera and occludes the region behind as shown in Fig. 1. By analyzing the appearance of a variety of raindrops, we found 4 features of raindrops: (i) the region of a raindrop has a different pixel intensity from neighbor regions, (ii) the region of a raindrop has monotonous variation of texture, (iii) the shape of a raindrop is approximated to an ellipse and (iv) the region of a raindrop is blurred. We detect raindrops in an image based on the above features by the 3 steps: (A) raindrop candidate detection using MSER, (B) evaluation using ellipse fitting and (C) evaluation using 2D Gaussian fitting. The detail of each step is described in the following.

### (A) Raindrop candidate detection using MSER

We employ the image segmentation method using MSER [13] to detect raindrop candidates from an image. In the conventional methods [8], [9], the SURF feature detector is



Fig. 1. Example of adherent raindrops: (a) original image and (b) enlarged view of the red-colored region in (a).



Fig. 2. Image segmentation using MSER for finding raindrop candidates: (a) original image and (b) MSERs with colored labels.

used to detect raindrop candidates. However, SURF does not always find all the raindrops from the image and the number of missed detections of SURF is more than that of MSER.

We generate contiguous binarized images from the input grayscale image by changing the threshold  $th$  from 0 to 255 (or from 255 to 0). As a result, all the pixels in a sequence of binarized images vary from white to black (or from black to white). Some white regions (or black regions) are observed in the process of changing the binarization threshold. Let  $Q_1, Q_2, \dots, Q_{th}, \dots$  be a sequence of extremal regions. MSER  $Q_{th^*}$  is obtained with the threshold  $th^*$  which is defined by

$$th^* = \arg \min_{th} |Q_{th+\Delta} \setminus Q_{th-\Delta}| / |Q_{th}|, \quad (1)$$

where  $Q_{th+\Delta} \setminus Q_{th-\Delta}$  is a difference set between  $Q_{th+\Delta}$  and  $Q_{th-\Delta}$ ,  $|Q_{th}|$  is an area of  $Q_{th}$  and  $\Delta$  is a parameter.

Fig. 2 shows an example of detected MSERs with a colored label. The detected MSERs satisfy features (i) and (ii), while there are a lot of false detections observed as shown in Fig. 2 (b). In the following steps, we identify the regions satisfying features (iii) and (iv) from the detected MSERs.

### (B) Evaluation using ellipse fitting

We select the regions satisfying feature (iii) from the candidates by ellipse fitting. Consider the MSER  $Q$ , where the number of pixels in  $Q$  is  $N$  and the pixel coordinate in  $Q$  is  $\mathbf{m}_i = [x \ y]^T$  ( $1 \leq i \leq N$ ). First, the covariance matrix  $\Sigma$  of

$Q$  is calculated by

$$\Sigma = \frac{1}{N-1} \sum_{i=1}^N (\mathbf{m}_i - \boldsymbol{\mu})(\mathbf{m}_i - \boldsymbol{\mu})^T, \quad (2)$$

where  $\boldsymbol{\mu}$  is a mean of pixel coordinates defined by

$$\boldsymbol{\mu} = [\mu_x \ \mu_y]^T = \frac{1}{N} \sum_{i=1}^N \mathbf{m}_i. \quad (3)$$

The direction of major and minor axes is obtained from the eigen vectors of the covariance matrix  $\Sigma$ . The length of the major axis,  $ma$ , and the minor axis,  $mi$ , is defined by the length from end to end in  $Q$  for each axis.

Next, we evaluate ellipse fitting by F-measure [14] between  $Q$  and the ellipse. The F-measure  $F$  is defined by the harmonic mean of precision and recall which considers the area ratio of the ellipse within  $Q$  and the area ratio of  $Q$  within the ellipse. The ellipse and  $Q$  are completely overlapped if the F-measure is 1. We select the regions from the candidates  $Q$  which satisfy the following condition:

$$F > th_1 \text{ and } \frac{ma}{mi} > th_2. \quad (4)$$

Note that we introduce  $th_2$  to remove the candidate whose shape likes a line.

### (C) Evaluation using 2D Gaussian fitting

We select the regions satisfying feature (iv) from the candidates by 2D Gaussian fitting. Fig. 3 shows the shape of pixel intensities of raindrops. The shape of raindrops is classified into 2 types such as Fig. 3 (c) and (d) from our empirical observation. In the case of Fig. 3 (c), the region has a high pixel intensity and is blurred, i.e., the shape is convex upward. In the case of Fig. 3 (d), the region has a low pixel intensity and is blurred, i.e., the shape is convex downward. In other cases such as Fig. 3 (e) and (f), the pixel intensities are randomly distributed. Hence, we employ 2D Gaussian fitting to identify raindrops, e.g., Fig. 3 (c) and (d), from the candidates  $Q$ . A 2D Gaussian can be used to model an arbitrary convex shape with parameters such as the center, variance and rotation. To address a raindrop widely spread, we also employ a logarithm of a 2D Gaussian for modeling the raindrop.

First, the pixel intensities in  $Q$  are normalized to [0 1] by

$$P(\mathbf{m}_i) = \frac{Q(\mathbf{m}_i) - Q_{\min}}{Q_{\max} - Q_{\min}}, \quad (5)$$

where  $P$  is a normalized MSER,  $Q_{\min}$  is the minimum intensity value in  $Q$  and  $Q_{\max}$  is the maximum intensity value in  $Q$ .

Next, the shape of  $P$  is normalized so as to be convex upward by

$$P(\mathbf{m}_i) = \begin{cases} P(\mathbf{m}_i) & \mu(P_{inner}) < \mu(P_{outer}) \\ 1 - P(\mathbf{m}_i) & \text{otherwise} \end{cases}, \quad (6)$$

where  $\mu(P_{inner})$  indicates a mean of pixel intensities around the center of  $P$  and  $\mu(P_{outer})$  indicates a mean of pixel intensities around the boundary of  $P$ .

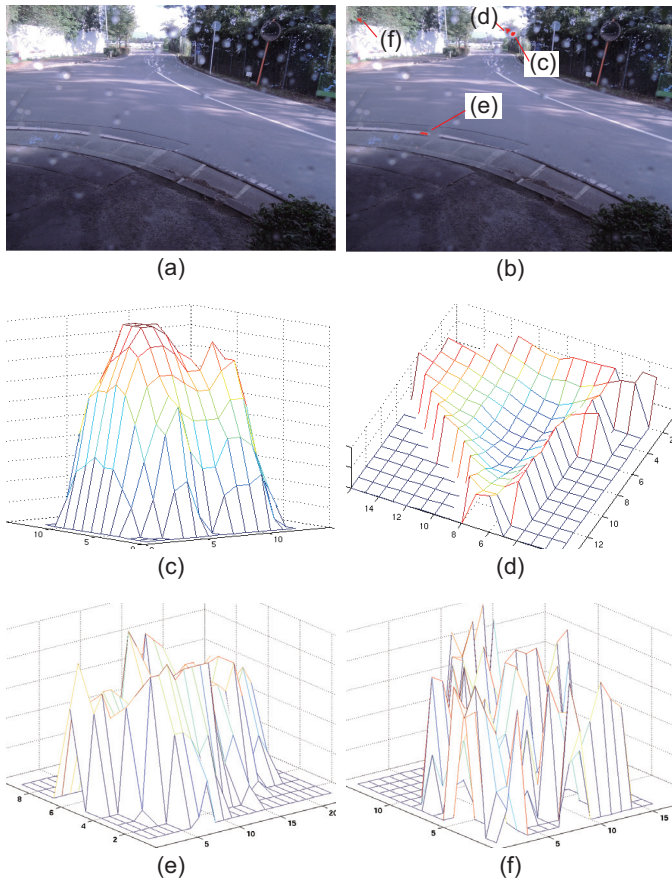


Fig. 3. The shape of pixel intensities in raindrop candidates: (a) original image, (b) examples of detected raindrop candidates by MSER, (c) and (d) the shape of pixel intensities on a raindrop and (e) and (f) the shape of pixel intensities on other region.

Then, a 2D Gaussian  $G(\mathbf{m}_i)$  is fitted to the normalized MSER  $P$ , which is defined by

$$G(\mathbf{m}_i) = \frac{1}{2\pi|\Sigma'|^{\frac{1}{2}}} \exp\left(-\frac{1}{2}(\mathbf{m}_i - \boldsymbol{\mu}')^T \Sigma'^{-1}(\mathbf{m}_i - \boldsymbol{\mu}')\right), \quad (7)$$

where  $\boldsymbol{\mu}'$  is a mean of pixel coordinates in  $P$  calculated by

$$\boldsymbol{\mu}' = [\mu'_x \ \mu'_y] = \frac{1}{N} \sum_{i=1}^N \mathbf{m}_i. \quad (8)$$

$\Sigma'$  indicates a covariance matrix defined by

$$\Sigma' = \begin{bmatrix} \sigma_x^2 & \rho\sigma_x\sigma_y \\ \rho\sigma_x\sigma_y & \sigma_y^2 \end{bmatrix}, \quad (9)$$

where  $\sigma_x^2$  and  $\sigma_y^2$  indicate variances for  $x$ - and  $y$ -axes, respectively,  $\rho$  indicates a correlation coefficient between  $x$  and  $y$ . The pixel intensities of  $G(\mathbf{m}_i)$  are also normalized to  $[0 \ 1]$  as well as  $Q$ . In addition, we calculate a logarithm of  $G(\mathbf{m}_i)$  by

$$\hat{G}(\mathbf{m}_i) = \ln\{G(\mathbf{m}_i)\}. \quad (10)$$

The pixel intensities of  $\hat{G}(\mathbf{m}_i)$  are also normalized to  $[0 \ 1]$ .

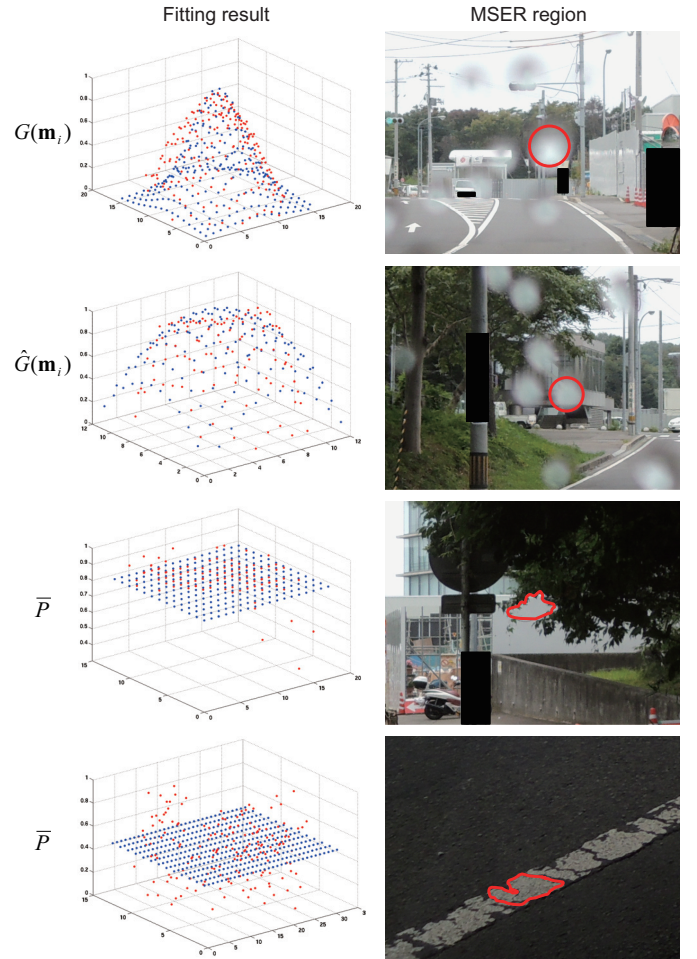


Fig. 4. Results of 2D Gaussian fitting for raindrop candidates.

Finally, we select the candidates  $P$  as raindrops if  $P$  satisfies the following condition:

$$\sum_{i=1}^N (P(\mathbf{m}_i) - G(\mathbf{m}_i))^2 < \sum_{i=1}^N (P(\mathbf{m}_i) - \bar{P})^2 \quad \text{or} \quad \sum_{i=1}^N (P(\mathbf{m}_i) - \hat{G}(\mathbf{m}_i))^2 < \sum_{i=1}^N (P(\mathbf{m}_i) - \bar{P})^2, \quad (11)$$

where  $\bar{P}$  is a mean of pixel intensities of  $P$ .

Fig. 4 shows examples of  $P$  fitted to  $G(\mathbf{m}_i)$ ,  $\hat{G}(\mathbf{m}_i)$  and  $\bar{P}$ , respectively. The red-colored points indicate  $P(\mathbf{m}_i)$  and the blue-colored points indicate a fitted function. The raindrops such as Fig. 3 (c) and (d) are well fitted to  $G(\mathbf{m}_i)$  and  $\hat{G}(\mathbf{m}_i)$ , while other regions such as Fig. 3 (e) and (f) are fitted to the plane  $\bar{P}$ .

Through the steps from (A) to (C), we can detect raindrops from a single image.

### III. EXPERIMENTS AND DISCUSSION

This section describes the performance evaluation of the proposed method using the images with adherent raindrops.

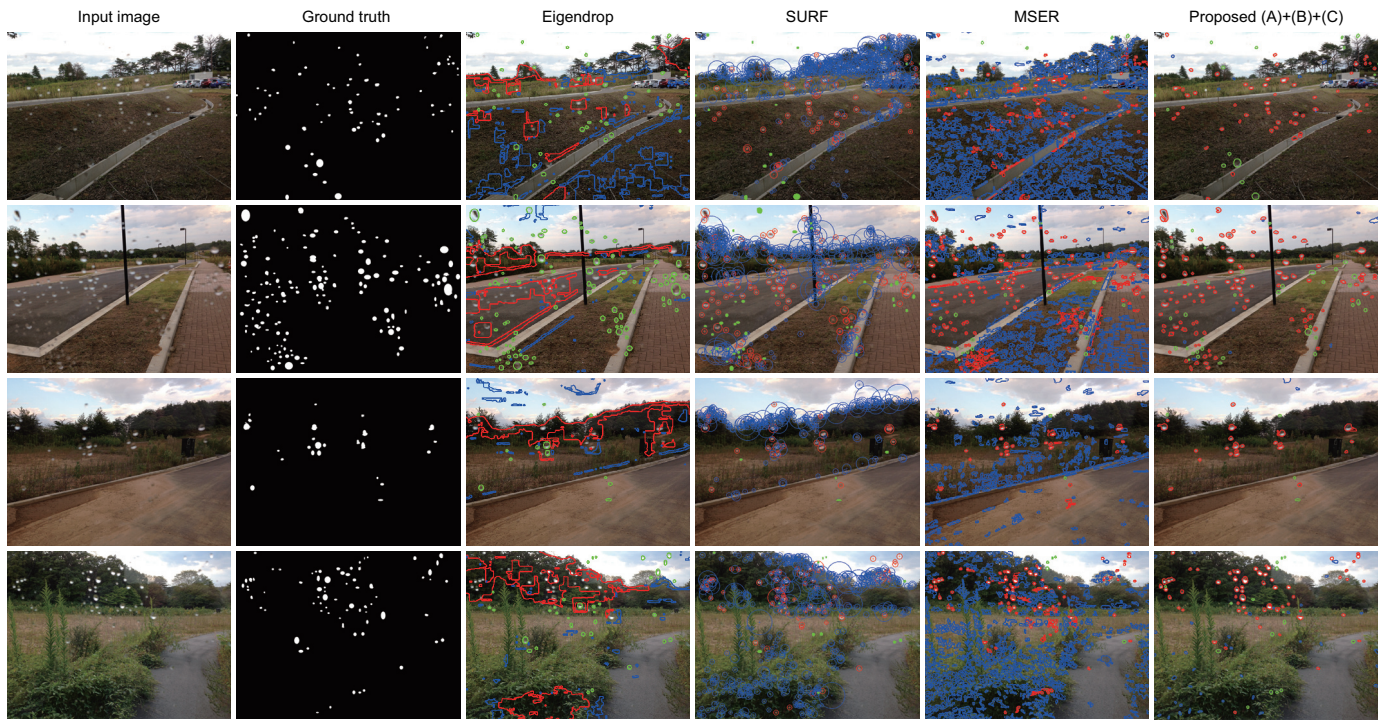


Fig. 5. Results of raindrop detection using the conventional and proposed methods, where the red-colored region indicates the region having raindrops, the blue-colored region indicates false detection and the green-colored region indicates missed detection.

An acrylic board is located in front of a camera, where the distance between the camera and the board is 10~20cm, waterdrops are adhered to the acrylic board and 13 images are taken by the camera, where 9 images are used in training for conventional methods and 4 images are used in testing for all the methods. We evaluate missed detection rates and false detection rates of the raindrop detection methods. In this experiment, we compare the accuracy of the proposed method with that of Eigendrop [6] and SURF [8]. Eigendrop is created by 9 training images, where about 100 raindrops are included in each image. In the proposed method, we employ parameters for Eq. (7):  $th_1 = 0.8$  and  $th_2 = 3$ .

Fig. 5 shows input images, ground truth data of raindrops, detection results of the conventional and proposed methods, where the ground truth data is manually created. The red-colored region indicates the region having raindrops, the blue-colored region indicates false detection and the green-colored region indicates missed detection. Eigendrop has a lot of missed regions compared with SURF and MSER, and SURF has more missed regions than MSER. As a result, MSER exhibits efficient performance for finding raindrop candidates compared with other methods. The proposed method (A)+(B)+(C) selects correct raindrops from results of image segmentation using MSER.

Table I summarizes missed and false detection rates for each method. To confirm performance of each step in the proposed method, we compare the accuracy of a variety of the proposed methods such as (A), (A)+(B), (A)+(C), (A)+(B)+(C) and (A)+(C)+(B). Eigendrop has high missed detection rate and

high false detection rate compared with other methods, since the accuracy is heavily depending on the training data. SURF exhibits better performance than Eigendrop, while the missed detection rate of SURF is significantly higher than (A) MSER. The missed detection rate is almost the same in a variety of the proposed methods, since the steps (B) and (C) exhibit efficient performance to remove candidates which do not include any raindrop. The combined use of the steps (B) and (C) makes it possible to improve the false detection rates.

As observed above, the proposed method can detect almost all raindrops in the image from the single image, although the proposed method does not need training data, video sequences and special devices to detect raindrops in the image. After detecting raindrops using the proposed method, we will remove detected raindrops using the inpainting technique [15]. In addition, we confirmed that the proposed method exhibits efficient performance of adherent raindrop detection in practical situations such as a large amount of video sequences taken by an in-vehicle camera. These results cannot be included in this paper due to limitations of space.

#### IV. CONCLUSION

This paper proposed an adherent raindrop detection method using MSER. The proposed method employs qualitative metrics to detect adherent raindrops from the result of MSER-based image segmentation. Through a set of experiments, we demonstrated that the proposed method exhibits efficient performance of adherent raindrop detection compared with the conventional methods.

TABLE I  
SUMMARY OF MISSED DETECTION RATES AND FALSE DETECTION RATES  
FOR EACH METHOD.

	Method	Missed rate	False rate
Image 1	Eigendrop	66.7%	98.2%
	SURF	62.3%	86.0%
	MSER (A)	7.2%	83.2%
	(A)+(B)	14.5%	42.2%
	(A)+(C)	20.3%	15.7%
	(A)+(B)+(C)	21.7%	6.6%
Image 2	(A)+(C)+(B)	21.7%	6.6%
	Eigendrop	68.3%	92.9%
	SURF	39.4%	74.8%
	MSER (A)	11.3%	51.2%
	(A)+(B)	21.1%	12.7%
	(A)+(C)	22.5%	8.1%
Image 3	(A)+(B)+(C)	26.0%	2.5%
	(A)+(C)+(B)	26.0%	2.5%
	Eigendrop	50.0%	96.4%
	SURF	54.2%	53.8%
	MSER (A)	12.5%	72.5%
	(A)+(B)	16.7%	21.4%
Image 4	(A)+(C)	16.7%	14.4%
	(A)+(B)+(C)	16.7%	3.2%
	(A)+(C)+(B)	16.7%	3.2%
	Eigendrop	47.3%	96.9%
	SURF	33.8%	46.9%
	MSER (A)	6.8%	79.6%
Image 4	(A)+(B)	20.3%	44.3%
	(A)+(C)	18.9%	31.8%
	(A)+(B)+(C)	21.6%	22.4%
	(A)+(C)+(B)	22.4%	21.6%

REFERENCES

[1] W. Hu, T. Tan, L. Wang, and S. Maybank, "A survey on visual surveillance of object motion and behaviors," *IEEE Trans. Syst. Man. Cybern. C*, vol. 34, no. 3, pp. 334–352, Aug. 2004.

[2] K. Garg and S.K. Nayar, "Detection and removal of rain from videos," *Proc. IEEE Computer Society Conf. Computer Vision and Pattern Recognition*, vol. 1, pp. I-528–I-535, 2004.

[3] X. Zhang, H. Li, Y. Qi, W.K. Leow, and T.K. Ng, "Rain removal in video by combining temporal and chromatic properties," *Proc. IEEE Int'l Conf. Multimedia and Expo*, pp. 461–464, 2006.

[4] P.C. Barnum, S. Narashimhan, and T. Kanade, "Analysis of rain and snow in frequency space," *Int'l J. Computer Vision*, vol. 86, no. 2–3, pp. 256–274, Jan. 2010.

[5] L. Kang, C. Lin, and Y. Fu, "Automatic single-image-based rain streaks removal via image decomposition," *IEEE Trans. Image Processing*, vol. 21, no. 4, pp. 1742–1755, 2012.

[6] H. Kurihata, T. Takahashi, I. Ide, Y. Mekada, H. Murase, and Y. Tamatsu, "Rainy weather recognition from in-vehicle camera images for driver assistance," *Proc. IEEE Intelligent Vehicles Symp.*, pp. 205–210, 2005.

[7] Q. Wu, W. Zhang, and B.V.K. Vijayakumar, "Raindrop detection and removal using salient visual features," *Proc. IEEE Int'l Conf. Image Processing*, pp. 941–944, 2012.

[8] J.C. Halimeh and M. Roser, "Raindrop detection on car windshields using geometric-photometric environment construction and intensity-based correlation," *Proc. IEEE Intelligent Vehicles Symp.*, pp. 610–615, 2009.

[9] M. Roser and A. Geiger, "Video-based raindrop detection for improved image registration," *Proc. IEEE Int'l Conf. Computer Vision Workshops*, pp. 570–577, 2009.

[10] S. You, R.T. Tan, R. Kawakami, and K. Ikeuchi, "Adherent raaindrop detection and removal in video," *Proc. IEEE Computer Society Conf. Computer Vision and Pattern Recognition*, pp. 1035–1042, June 2013.

[11] A. Yamashita, Y. Tanaka, and T. Kaneko, "Removal of adherent waterdrops from images acquired with stereo camera," *Proc. IEEE/RSJ Int'l Conf. Intelligent Robots and Systems*, pp. 400–405, Aug. 2005.

[12] AA. Yamashita, I. Fukuchi, and T. Kaneko, "Noises removal from image sequences acquired with moving camera by estimating camera motion from spatio-temporale information," *Proc. IEEE/RSJ Int'l Conf. Intelligent Robots and Systems*, pp. 3794–3801, Oct. 2009.

[13] J. Matas, O. Chum, M. Urban, and T. Pajdla, "Robust wide-baseline stereo from maximally stable extremal regions," *Image and Vision Computing*, vol. 22, no. 10, pp. 761–767, 2004.

[14] N. Chinchor, "MUC-4 evaluation metrics," *Proc. Conf. Message understanding*, pp. 22–29, 1992.

[15] M. Bertalmio, G. Sapiro, V. Caselles, and C. Ballester, "Image inpainting," *Proc. Annual Conf. Computer Graphics and Interactive Techniques*, pp. 417–424, 2000.